Inverse Problems and Imaging
Volume 7, No. 2, 2013, x–xx
doi:10.3934/ipi.2013.7.xx

STUDY OF NOISE EFFECTS IN ELECTRICAL IMPEDANCE TOMOGRAPHY WITH RESISTOR NETWORKS

Liliana Borcea

Computational and Applied Mathematics, Rice University
MS 134, 6100 Main St. Houston, TX 77005-1892, USA

Fernando Guevara Vasquez

Department of Mathematics, University of Utah
155 S 1400 E RM 233, Salt Lake City, UT 84112-0090, USA

Alexander V. Mamonov

Institute for Computational Engineering and Sciences
University of Texas at Austin
1 University Station C0200, Austin, TX 78712, USA

(Communicated by Matti Lassas)

Abstract. We present a study of the numerical solution of the two dimensional electrical impedance tomography problem, with noisy measurements of the Dirichlet to Neumann map. The inversion uses parametrizations of the conductivity on optimal grids. The grids are optimal in the sense that finite volume discretizations on them give spectrally accurate approximations of the Dirichlet to Neumann map. The approximations are Dirichlet to Neumann maps of special resistor networks, that are uniquely recoverable from the measurements. Inversion on optimal grids has been proposed and analyzed recently, but the study of noise effects on the inversion has not been carried out. In this paper we present a numerical study of both the linearized and the nonlinear inverse problem. We take three different parametrizations of the unknown conductivity, with the same number of degrees of freedom. We obtain that the parametrization induced by the inversion on optimal grids is the most efficient of the three, because it gives the smallest standard deviation of the maximum a posteriori estimates of the conductivity, uniformly in the domain. For the nonlinear problem we compute the mean and variance of the maximum a posteriori estimates of the conductivity, on optimal grids. For small noise, we obtain that the estimates are unbiased and their variance is very close to the optimal one, given by the Cramér-Rao bound. For larger noise we use regularization and quantify the trade-off between reducing the variance and introducing bias in the solution. Both the full and partial measurement setups are considered.

1. **Introduction .** We study the inverse problem of electrical impedance tomography (EIT) in two dimensions, with noisy measurements of the Dirichlet to Neumann (DtN) map. Explicitly, we seek the positive and bounded, scalar valued coefficient $\sigma(\mathbf{x})$ in the elliptic equation

$$\nabla \cdot [\sigma(\mathbf{x}) \nabla u(\mathbf{x})] = 0, \qquad \mathbf{x} \in \Omega. \tag{1}$$

2010 *Mathematics Subject Classification.* Primary: 35R30, 35J15.
Key words and phrases. Electrical impedance tomography, resistor networks, parametrization.

The domain Ω is bounded, simply connected, with smooth boundary $\mathcal{B}$. By the Riemann mapping theorem all such domains in $\mathbb{R}^2$ are conformally equivalent. In this work we consider the domains for which the corresponding conformal mapping is smooth up to the boundary [35]. So from now on we take for Ω the unit disk. We call $\sigma(\mathbf{x})$ the conductivity and $u \in H^1(\Omega)$ the potential, satisfying the boundary conditions

$$u(\mathbf{x}) = V(\mathbf{x}), \qquad \mathbf{x} \in \mathcal{B}, \tag{2}$$

for arbitrary $V \in H^{1/2}(\mathcal{B})$. The data are finitely many noisy measurements of the DtN map $\Lambda_\sigma : H^{1/2}(\mathcal{B}) \to H^{-1/2}(\mathcal{B})$, which takes the boundary potential V to the normal boundary flux (current)

$$\Lambda_\sigma V(\mathbf{x}) = \sigma(\mathbf{x}) \frac{\partial u(\mathbf{x})}{\partial n}, \qquad \mathbf{x} \in \mathcal{B}. \tag{3}$$

We consider both the *full boundary* setup, where $\Lambda_\sigma V$ is measured all around the boundary $\mathcal{B}$, and the *partial boundary* setup, where the measurements are confined to an accessible subset $\mathcal{B}_A \subset \mathcal{B}$, and the remainder $\mathcal{B}_I = \mathcal{B} \setminus \mathcal{B}_A$ of the boundary is assumed grounded ($V|_{\mathcal{B}_I} = 0$).

In theory, full knowledge of the DtN map Λ_σ determines uniquely σ, as proved in [34, 14] under some smoothness assumptions on σ, and in [5] for bounded σ. The result extends to the partial boundary setup, at least for $\sigma \in C^{3+\epsilon}(\bar{\Omega})$, $\epsilon > 0$ as established in [24]. In practice, the difficulty lies in the exponential instability of EIT. It is shown in [1, 7, 33] that the best possible stability estimate is of logarithmic type. Thus even if the noisy data is consistent (i.e. in the set of DtN maps) we need exponentially small noise to get a conductivity that is close to the true one.

It is shown in [2] that if σ has finitely many degrees of freedom, more precisely if it is piecewise constant with a bounded number of unknown values, then the stability estimates on σ are of Lipschitz type. However, it is not clear how the Lipschitz constant grows depending on the distribution of the unknowns in Ω. For example, it should be much easier to determine the value of σ near the boundary than in a small set in the interior of Ω.

An important question is how to find parametrizations of σ that capture the trade-off between stability and resolution as we move away from the boundary, where the measurements are made. On one hand, the parametrizations should be sparse, with a small number of degrees of freedom. On the other hand, the parametrizations should be adaptively refined toward the boundary.

Adaptive parametrizations for EIT have been proposed in [28, 31] and in [3, 4]. The first approaches use *distinguishability grids* that are defined with a linearization argument. The approach in [3, 4] is nonlinear and consists of an iterative coarsening and refinement of a piecewise constant discretization of the conductivity, with each discretization update being computationally costly.

We follow the approach in [9, 37, 12, 13] and parametrize σ on *optimal grids*. The number of parameters is limited by the noise level in the measurements and their geometrical distribution in Ω is determined as part of the inversion. The grids are based on rational approximations of the DtN map. We call them optimal because they give spectral accuracy of approximations of Λ_σ with finite volume schemes. The grids turn out to be refined near the accessible boundary, where we make the measurements, and coarse away from it, thus capturing the expected loss of resolution of the reconstructions of σ.

Optimal grids were introduced in [6, 20, 21, 26] for accurate approximations of the DtN map in forward problems. Inversion on optimal grids was first proposed for Sturm-Liouville inverse spectral problems in [8]. The analysis in [11] shows that optimal grids are necessary and sufficient for convergence of solutions of discrete inverse spectral problems to the true solution of the continuum one. The numerical solution of EIT on optimal grids was introduced in [9, 23] for the full boundary measurements case, and in [12, 13, 32] for partial boundary measurements. The inversion in [9, 23, 12, 13, 32] is based on the rigorous theory of discrete inverse problems for circular planar resistor networks [15, 16, 25, 18, 19], which gives networks that can be uniquely determined by discrete measurements of the continuum DtN map [27, 9]. Just as in the continuum EIT, the inverse problem for networks is ill-posed, and there is a trade-off between the size of the network and the stability of the reconstruction.

We present here a study of the inversion algorithms on optimal grids, for noisy measurements of the DtN map. We fix the number g of degrees of freedom, and analyze the effect of the adaptive parametrization of σ on the reconstruction error. We consider maximum a posteriori estimates of σ for the linearized problem about a constant conductivity, and for the nonlinear problem. The noise is mean zero Gaussian, and if its standard deviation is small, the only prior on σ is that it is positive and bounded. For larger noise we use regularization (Gaussian priors), and study how the parametrization affects the trade-off between the stability of the result and the bias.

We study three different parametrizations of σ, with g degrees of freedom. The first two are piecewise linear, on an equidistant grid and on the optimal grid. The only relation between the second parametrization and resistor network inversion on optimal grids is the location of the grid nodes. The third parametrization is that induced by the resistor network inversion.

In the linearization study we compute the standard deviation of the estimates and show that the resistor network parametrization is clearly superior. It gives estimates with uniformly small standard deviation in Ω. The conclusion is that it is not enough to distribute the parameters on the optimal grid to obtain good results. To control the stability of the reconstructions, we also need to use proper basis functions.

In the nonlinear statistical study we compute maximum a posteriori estimates of σ with the inversion algorithms on optimal grids. We assess their quality by displaying pointwise in Ω their mean and standard deviation. We obtain that the resistor network based inversion is efficient in the sense that it gives unbiased estimates of σ, with variance that is very close to the optimal Cramér-Rao bound [36]. This is for small noise. For larger noise we use regularization priors that introduce some bias in the solution. We also compare the network based inversion to the usual optimization approach that seeks the conductivity as the least squares minimizer of the data misfit. For the optimization, the conductivity is piecewise linear with the same number g of degrees of freedom, either on a uniform grid or on the optimal grid. Our numerical experiments indicate that for a fixed allowed error (standard deviation) in the reconstructions, the network based method gives reconstructions that are closer in average to the true conductivity (i.e. with less bias). The conclusion for the non-linear problem is similar to that for the linearized problem: the reconstruction error is reduced with the network based inversion as compared to

optimization on either equidistant or optimal grids. Our study considers both the full and partial measurement setups [9, 23, 12, 13, 32].

The paper is organized as follows: We begin in section 2 with the estimation framework. Then we review the resistor network inversion in section 3. The tools needed for the numerical experiments are described in section 4. The estimation results are in section 5. We end with a summary in section 6.

2. Maximum a posteriori estimation of the conductivity.

We study how different parametrizations of the unknown conductivity, with a fixed number g of degrees of freedom, affect the sensitivity of the reconstructions to noise in the data. Let $\mathbf{s} = (s_1, \ldots, s_g)^T \in \mathbb{R}^g$ be the vector of parameters, and

$$\sigma(\mathbf{x}) = [\mathcal{S}(\mathbf{s})](\mathbf{x}), \quad \mathbf{x} \in \bar{\Omega} \tag{4}$$

the parametrization of the reconstruction conductivity, using an operator $\mathcal{S} : \mathbb{R}^g \to C(\Omega)$ that takes $\mathbf{s}$ to a continuous function in Ω. Since the data is noisy, the reconstructions are random variables. We study maximum a posteriori estimates of the reconstructions under certain priors, as explained in section 2.1. We consider three different parametrizations of the form (4), outlined in section 2.2.

2.1. Estimation.

We denote by $\mathbf{F} : C(\Omega) \to \mathbb{R}^{n(n-1)/2}$, the forward map that associates to a conductivity σ the vector of measurements $\mathbf{F}(\sigma)$ of the DtN map. The measurement operation is explained in detail in section 3.1.1. It amounts to recording voltages and currents at n electrodes on the boundary. The dimension $n(n-1)/2$ of the data vector $\mathbf{d}$ corresponds to the number of independent measurements that can be made with n electrodes. From now on, we take the number of parameters of the unknown conductivity to be $g = n(n-1)/2$, so that we use the least number of parameters needed for taking into account all of the independent measurements. The data model is

$$\mathbf{d} = \mathbf{F}(\sigma) + \boldsymbol{\epsilon}, \qquad \boldsymbol{\epsilon} \in \mathcal{N}(\mathbf{0}, \mathcal{C}), \tag{5}$$

with $\boldsymbol{\epsilon}$ the noise vector. The notation $\mathcal{N}(\mathbf{0}, \mathcal{C})$ states that $\boldsymbol{\epsilon}$ is Gaussian (multivariate normal), with mean zero and diagonal covariance $\mathcal{C}$. We refer to section 3.1.1 for an explanation of the uncorrelation of the components of $\boldsymbol{\epsilon}$.

We parametrize the conductivity as in (4) with a vector $\mathbf{s} \in \mathbb{R}^g$, with $g = n(n-1)/2$ being the same dimension as the data space. Since the data $\mathbf{d}$ is tainted with noise, we treat $\mathbf{s}$ as a continuum random variable, and denote by $\boldsymbol{\pi}_{\text{pr}}(\mathbf{s})$ its prior probability density. The likelihood function $\boldsymbol{\pi}(\mathbf{d}|\mathbf{s})$ is the probability density of $\mathbf{d}$ conditioned to knowing $\mathbf{s}$. Given our Gaussian noise model, it takes the form

$$\boldsymbol{\pi}(\mathbf{d}|\mathbf{s}) = \frac{1}{(2\pi)^{g/2}|\mathcal{C}|^{1/2}} \exp\left[-\frac{1}{2}(\mathbf{F}(\mathcal{S}(\mathbf{s})) - \mathbf{d})^T \mathcal{C}^{-1} (\mathbf{F}(\mathcal{S}(\mathbf{s})) - \mathbf{d})\right], \tag{6}$$

where $|\mathcal{C}|$ is the determinant of the covariance $\mathcal{C}$. The estimation of $\mathbf{s}$ is based on the conditional (posterior) density $\boldsymbol{\pi}(\mathbf{s}|\mathbf{d})$. It is defined by Bayes' rule [36, 22]

$$\boldsymbol{\pi}(\mathbf{s}|\mathbf{d}) = \frac{\boldsymbol{\pi}(\mathbf{s}, \mathbf{d})}{\boldsymbol{\pi}(\mathbf{d})} = \frac{\boldsymbol{\pi}(\mathbf{d}|\mathbf{s})\boldsymbol{\pi}_{\text{pr}}(\mathbf{s})}{\boldsymbol{\pi}(\mathbf{d})}, \tag{7}$$

where $\boldsymbol{\pi}(\mathbf{s}, \mathbf{d})$ is the joint probability density of $(\mathbf{s}, \mathbf{d})$. The marginal

$$\boldsymbol{\pi}(\mathbf{d}) = \int_{\mathbb{R}^g} \boldsymbol{\pi}(\mathbf{s}, \mathbf{d})\boldsymbol{\pi}_{\text{pr}}(\mathbf{s}) d\mathbf{s} \tag{8}$$

is just a normalization that plays no role in the estimation. The prior density $\boldsymbol{\pi}_{\text{pr}}(\mathbf{s})$ may introduce a regularization in the inverse problem [29, Chapter 3]. The priors used in our study are summarized in Appendix A. They all ensure that the reconstructions $\sigma(\mathbf{x})$ are positive. It is possible to combine different priors by multiplying them together, provided the result is properly normalized.

We consider maximum a posteriori (MAP) estimates of the conductivity

$$\sigma_{\text{MAP}}(\mathbf{x}) = [\mathcal{S}(\mathbf{s}_{\text{MAP}})](\mathbf{x}), \tag{9}$$

which maximize the conditional probability density $\pi(\mathbf{s}|\mathbf{d})$. The vector $\mathbf{s}_{\text{MAP}}$ of parameters solves the optimization problem

$$\mathbf{s}_{\text{MAP}} = \arg\min_{\mathbf{s}\in\mathbb{R}^g} [\mathbf{F}(\mathcal{S}(\mathbf{s})) - \mathbf{d}]^T \mathcal{C}^{-1} [\mathbf{F}(\mathcal{S}(\mathbf{s})) - \mathbf{d}] - \log(\boldsymbol{\pi}_{\text{pr}}(\mathbf{s})). \tag{10}$$

The MAP estimates $\mathbf{s}_{\text{MAP}}$ are random, because they depend on the noise $\boldsymbol{\epsilon}$ in the measurements. To quantify their uncertainty, we approximate their variance using a large number M of independent samples $\mathbf{s}_{\text{MAP}}^{(m)}$, determined from (10) and data (5) with draws $\boldsymbol{\epsilon}^{(m)} \in \mathcal{N}(\mathbf{0}, \mathcal{C})$ of the noise,

$$\text{Var}[\mathbf{s}] \approx \frac{1}{M-1} \sum_{m=1}^{M} \left[\mathbf{s}_{\text{MAP}}^{(m)} - \langle \mathbf{s} \rangle\right]^2, \quad \langle \mathbf{s} \rangle \approx \frac{1}{M} \sum_{m=1}^{M} \mathbf{s}_{\text{MAP}}^{(m)}. \tag{11}$$

Then, we compare Var[$\mathbf{s}$] to the optimal variance, which is the right hand side in the Cramér-Rao bound [36, Corollary 5.23],

$$\mathbb{E}_{\mathbf{s}_\star}\{[\mathbf{s}_{\text{MAP}} - \mathbb{E}_{\mathbf{s}_\star}\{\mathbf{s}_{\text{MAP}}\}]^2\} \geq \mathbf{b}^T(\mathbf{s}_\star) \mathcal{I}^{-1}(\mathbf{s}_\star) \mathbf{b}(\mathbf{s}_\star). \tag{12}$$

The notation $\mathbb{E}_{\mathbf{s}_\star}$ indicates that the mean (expectation) depends on the true vector of parameters $\mathbf{s}_\star$. The bias factor $\mathbf{b}(\mathbf{s})$ is defined by

$$\mathbf{b}(\mathbf{s}) = \nabla \mathbb{E}_{\mathbf{s}}\{\mathbf{s}_{\text{MAP}}\}, \tag{13}$$

where ∇ denotes gradient with respect to $\mathbf{s}$, and $\mathcal{I}(\mathbf{s})$ is the Fischer information matrix [36, Section 2.3]. It measures how much information the data $\mathbf{d}$ carry about the parameter $\mathbf{s}_\star$. The Fisher matrix is in $\mathbb{R}^{g\times g}$, with entries

$$\mathcal{I}_{i,j}(\mathbf{s}) = \mathbb{E}_{\mathbf{s}}\left\{\partial_{s_i} \log \pi(\mathbf{d}|\mathbf{s})\, \partial_{s_j} \log \pi(\mathbf{d}|\mathbf{s})\right\}. \tag{14}$$

Since the likelihood $\pi(\mathbf{d}|\mathbf{s})$ is Gaussian, we obtain under the natural assumption that the noise covariance $\mathcal{C}$ is independent of $\mathbf{s}$, that

$$\mathcal{I}(\mathbf{s}) = D_{\mathbf{s}}\mathcal{S}(\mathbf{s})^T D_\sigma \mathbf{F}(\mathcal{S}(\mathbf{s}))^T \mathcal{C}^{-1} D_\sigma \mathbf{F}(\mathcal{S}(\mathbf{s})) D_{\mathbf{s}}\mathcal{S}(\mathbf{s}), \tag{15}$$

where $D_{\mathbf{s}}\mathcal{S}(\mathbf{s})$ is the Jacobian of $\mathcal{S}(\mathbf{s})$ evaluated at $\mathbf{s}$ and $D_\sigma \mathbf{F}(\sigma)$ is the Jacobian of $\mathbf{F}(\sigma)$ evaluated at σ. We take as the true $\mathbf{s}_\star$ the solution of the optimization problem (10), with noiseless data and upper/lower bound prior (42). The bias $\mathbf{b}(\mathbf{s}_\star)$ is approximated via Monte Carlo simulations, from a large sample of draws. The bound (12) is evaluated and displayed in section 5.2.

2.2. **Parametrizations of the conductivity.** We consider three different parametrizations:

- **piecewise linear on uniform grid**: The entries in $\mathbf{s}$ are pointwise values of $\sigma(\mathbf{x})$ on a uniform tensor product grid. The conductivity is piecewise linear on a Delaunay triangulation of the grid points.
- **piecewise linear on optimal grid**: The conductivity and the parameters are defined as above, but with grid points from the so-called "optimal grid" (see section 3.2.1).

- **resistor network**: The parameters $\mathbf{s}$ are (up to known multiplicative constants) the conductors in a network that has the same electrical response (DtN map) as the electrical response at the electrodes of the unknown conductivity. This parametrization is discussed in more detail in section 2.3.

In the first two parametrizations the conductivity depends *linearly* on $\mathbf{s}$. It is the piecewise linear interpolation of the entries in $\mathbf{s}$, between grid nodes $\mathbf{x}_1, \ldots, \mathbf{x}_g$,

$$\sigma(\mathbf{x}) = [\mathcal{S}(\mathbf{s})](\mathbf{x}) = \sum_{i=1}^{g} s_i \phi_i(\mathbf{x}). \tag{16}$$

Here ϕ_i are piecewise linear basis functions on a Delaunay triangulation of the nodes $\mathbf{x}_i$, satisfying the usual property $\phi_i(\mathbf{x}_j) = \delta_{ij}$, with the Kronecker delta notation.

In the resistor network parametrization the conductivity depends *nonlinearly* on the parameters $\mathbf{s}$. The dependence is given in equation (19), in terms of the resistor network reduced model of (1). We emphasize that the resistor network parametrization cannot be written in the form (16). One way of comparing it to the linear case (16) is to consider a small perturbation $\delta\mathbf{s} \equiv (\delta s_1, \ldots, \delta s_g)^T$ of some reference $\bar{\mathbf{s}}$, and linearize

$$[\mathcal{S}(\bar{\mathbf{s}} + \delta\mathbf{s})](\mathbf{x}) = [\mathcal{S}(\bar{\mathbf{s}})](\mathbf{x}) + \sum_{i=1}^{g} \delta s_i \phi_i(\mathbf{x}) + o(\delta\mathbf{s}). \tag{17}$$

Here the ϕ_i are the "columns" of the Jacobian $D_{\mathbf{s}}\mathcal{S}(\bar{\mathbf{s}})$ of the parametrization operator $\mathcal{S}$ with respect to $\mathbf{s}$, and evaluated at $\bar{\mathbf{s}}$. We call these ϕ_i *sensitivity basis functions*.

2.3. The resistor network discretization and the sensitivity basis functions.

For a given resistor network with n boundary nodes and $g = n(n-1)/2$ resistors (one per edge), we denote by $\mathbb{F} : \mathbb{R}^g_+ \to \mathbb{R}^g$ the discrete forward map which maps the vector of positive conductances of the network to a vector of g independent entries of the Dirichlet-to-Neumann map of the network. The choice and ordering of the independent entries is identical to that of $\mathbf{F}$ in section 2.1. We assume that the topology (underlying graph) of the network is such that $\mathbb{F}$ admits a left inverse $\mathbb{F}^{-1}$, i.e. $\mathbb{F}^{-1}(\mathbb{F}(\boldsymbol{\gamma})) = \boldsymbol{\gamma}$ for all $\boldsymbol{\gamma} > 0$. Such topologies are given in section 3.1.2.

In the resistor network parametrization we let

$$\mathbf{s} = (\gamma_1/\gamma_1^{(1)}, \ldots, \gamma_g/\gamma_g^{(1)})^T \in \mathbb{R}^g_+.$$

Here the γ_i are the conductances of the network that has the same electrical response as that measured for σ, i.e. $\mathbf{F}(\sigma) = \mathbb{F}(\boldsymbol{\gamma})$, for $\boldsymbol{\gamma} = (\gamma_1, \ldots, \gamma_g)^T$. Similarly, $\boldsymbol{\gamma}^{(1)} = (\gamma_1^{(1)}, \ldots, \gamma_g^{(1)})^T$ satisfies $\mathbf{F}(1) = \mathbb{F}(\boldsymbol{\gamma}^{(1)})$. Hence, it is easy to compute $\mathbf{s}$ from knowledge of σ and $\mathbb{F}^{-1}$.

The mapping $\mathcal{S}$ in the resistor network parametrization is defined implicitly by

$$\mathbf{F}(\mathcal{S}(\mathbf{s})) = \mathbb{F}(\mathbf{s}\boldsymbol{\gamma}^{(1)}), \tag{18}$$

where the product of the vectors $\mathbf{s}$ and $\boldsymbol{\gamma}^{(1)}$ is understood componentwise. There are many functions that satisfy (18). We define $\mathcal{S}(\mathbf{s})$ for the resistor network parametrization as the limit of the Gauss-Newton sequence $\{\kappa_j\}_{j\geq 0}$ defined in (35),

$$[\mathcal{S}(\mathbf{s})](\mathbf{x}) = \exp(\kappa(\mathbf{x})), \quad \text{where } \kappa = \lim_{j\to\infty} \kappa_j. \tag{19}$$

The starting point in the Gauss-Newton iteration is $\kappa_o(\mathbf{x}) = \ln(\sigma^o(\mathbf{x}))$, where $\sigma^o(\mathbf{x})$ is the piecewise linear interpolation of the discrete values $\mathbf{s}$ on the optimal grid defined in section 3.2.1. In practice, the evaluation of (19) is computationally efficient because iteration (35) converges quickly, basically after one step, as shown in [9, 23].

Recall that for the resistor network parametrization, the mapping $\mathcal{S}$ is non-linear and thus cannot be written as an expansion in basis of functions, as in (16). To compare it to parametrizations of the form (16), we look at its linearization around reference parameters $\overline{\mathbf{s}}$ to obtain (17). The basis functions ϕ_k are then the "columns" of $D_{\mathbf{s}}\mathcal{S}(\overline{\mathbf{s}})$, which can be determined by differentiating (18) with respect to $\mathbf{s}$,

$$D_{\mathbf{s}}\mathcal{S}(\overline{\mathbf{s}}) = D_\sigma \mathbf{F}^\dagger(\mathcal{S}(\overline{\mathbf{s}}))D_{\boldsymbol{\gamma}}\mathbb{F}(\overline{\mathbf{s}}\boldsymbol{\gamma}^{(1)})\mathrm{diag}(\boldsymbol{\gamma}^{(1)}) = (\mathrm{diag}(1/\boldsymbol{\gamma}^{(1)})D_\sigma\boldsymbol{\gamma})^\dagger. \tag{20}$$

The sensitivity functions $D_\sigma\boldsymbol{\gamma}(\mathbf{x})$ are defined in section 3.2.1 and are evaluated at $\overline{\sigma} = \mathcal{S}(\overline{\mathbf{s}})$. They give the sensitivity of the resistors $\boldsymbol{\gamma}$ to changes in the conductivity, and are an important ingredient of the inversion algorithm that is reviewed in section 3.

2.4. **Outline of the results.** The linearized problem is studied in section 5.1. In this case it it is known [36, Section 5.1] that the Cramér-Rao bound is attained by the variance of the MAP estimates. The variance depends of course on the parametrization (4) used in the estimation. The results say that when we take piecewise linear interpolations of the parameters $\mathbf{s}$ on the equidistant or the optimal grids, we obtain much larger variances than if we use the sensitivity basis functions. That is to say, the sensitivity basis functions lead to better estimates than the piecewise linear ones, even when we interpolate on the optimal grids. We also show in section 5.2 that the nonlinear estimation based on resistor networks is efficient, in the sense that the sample variance is very close to the Cramér-Rao bound.

3. EIT with resistor networks.

The resistor networks used in our inversion algorithms are reduced models of (1) that are uniquely recoverable from discrete measurements of the continuum DtN map, as described in section 3.1. They allow us to estimate the conductivity σ parametrized on optimal grids, as explained in section 3.2. We give here a brief summary of the measurement operation, the critical resistor networks, and the induced reconstruction mapping (19) used in this paper. We refer to [9, 12, 13] for more details of the resistor network based inversion.

3.1. **Resistor networks as reduced models for the forward and inverse problem.** Resistor networks arise naturally in finite volume discretizations of equation (1) on staggered grids with interlacing primary and dual grid lines that may be curvilinear. The potential is discretized at the primary nodes $P_{i,j}$, the intersections of the primary grid lines, $u_{i,j} \approx u(P_{i,j})$. Each node $P_{i,j} \in \Omega$ is surrounded by a dual cell $C_{i,j}$, as shown in Figure 1. Integrating (1) over the cells $C_{i,j}$, using the divergence theorem, and approximating the boundary fluxes with finite differences we obtain a system of linear equations of the form

$$\begin{aligned} &\gamma_{i+\frac{1}{2},j}(u_{i+1,j} - u_{i,j}) + \gamma_{i-\frac{1}{2},j}(u_{i-1,j} - u_{i,j}) \\ &+\gamma_{i,j+\frac{1}{2}}(u_{i,j+1} - u_{i,j}) + \gamma_{i,j-\frac{1}{2}}(u_{i,j-1} - u_{i,j}) = 0. \end{aligned} \tag{21}$$

Equations (21) are Kirchhoff's node law for the interior nodes of the resistor network with graph $\Gamma = (\mathcal{P}, \mathcal{E})$. Here $\mathcal{P} = \{P_{i,j}\}$ is the set of primary nodes, given by the union of the disjoint sets $\mathcal{P}_{\mathcal{B}}$ and $\mathcal{P}_{\mathcal{I}}$ of boundary and interior nodes. Adjacent primary nodes are connected by edges, the elements of the set $\mathcal{E} \subset \mathcal{P} \times \mathcal{P}$.

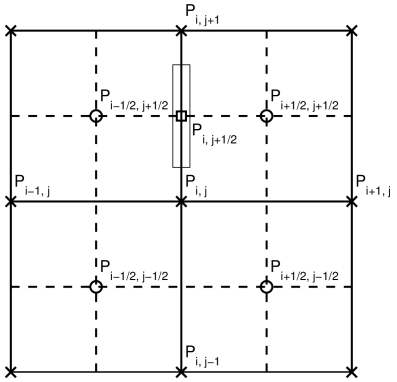

FIGURE 1. Illustration of a staggered grid, with primary (solid) and dual (dashed) grid lines. The primary grid nodes are indicated by $\times$ and the dual grid nodes by $\circ$. We show a resistor as a rectangle with a midpoint $\square$ at the intersection of a primary and dual line.

The network is the pair $(\Gamma, \boldsymbol{\gamma})$, with $\boldsymbol{\gamma} \in \mathbb{R}_+^{|\mathcal{E}|}$ the vector with entries given by the conductances (inverse of resistances) $\gamma_{\alpha,\beta} > 0$ of the edges, following a preassigned ordering of $\mathcal{E}$. Here $(\alpha, \beta) \in \left\{\left(i, j \pm \frac{1}{2}\right),\ \left(i \pm \frac{1}{2}, j\right)\right\}$.

We relate the conductances $\gamma_{\alpha,\beta}$ and σ by

$$\gamma_{\alpha,\beta} = \sigma(P_{\alpha,\beta}) \frac{L(\Sigma_{\alpha,\beta})}{L(E_{\alpha,\beta})}, \tag{22}$$

where L denotes the arclengths of the primary edges $E_{\alpha,\beta}$ and dual edges $\Sigma_{\alpha,\beta}$. The points $P_{\alpha,\beta}$ are located at the intersections of the primary and dual grid segments $E_{\alpha,\beta}$ and $\Sigma_{\alpha,\beta}$.

The *forward problem* for a known network $(\Gamma, \boldsymbol{\gamma})$ amounts to determining the potential function $\mathcal{U} : \mathcal{P} \to \mathbb{R}$, with $u_{i,j} = \mathcal{U}(P_{i,j})$ satisfying the conservation of currents (21) at the interior nodes, and Dirichlet boundary conditions

$$u|_{\mathcal{P}_\mathcal{B}} = u_\mathcal{B}. \tag{23}$$

We denote the number of boundary nodes by n. The entries in the vector $u_\mathcal{B} \in \mathbb{R}^n$ may be related to the continuum boundary potential V as explained below, in section 3.1.1.

The *inverse problem* for the network seeks the conductances $\boldsymbol{\gamma}$ from the discrete DtN map $\Lambda_{\boldsymbol{\gamma}}$. The graph Γ is known, and the DtN map is a matrix in $\mathbb{R}^{n\times n}$ that maps the vector $u_\mathcal{B}$ of boundary potentials to the vector $J_\mathcal{B}$ of boundary current fluxes. Since we consider the two dimensional problem, all the graphs Γ are *circular planar graphs* [15, 16], i.e. graphs that can be embedded in the plane with no crossing edges and with all boundary nodes $\mathcal{P}_\mathcal{B}$ lying on a circle.

3.1.1. ***Discrete measurements of the continuum DtN map.*** To connect the discrete inverse problem for the network $(\Gamma, \boldsymbol{\gamma})$ to continuum EIT, we introduce a *measurement operator* $\mathcal{M}_n$ that defines a matrix $\mathcal{M}_n(\Lambda_\sigma) \in \mathbb{R}^{n\times n}$ from the continuum DtN map Λ_σ. The measurement operator is chosen so that for any suitable conductivity, $\mathcal{M}_n(\Lambda_\sigma)$ is *consistent* with the DtN map of a circular planar resistor network $(\Gamma, \boldsymbol{\gamma})$. The network is a reduced model for the forward problem,

because it satisfies

$$\Lambda_{\boldsymbol{\gamma}} = \mathcal{M}_n\left(\Lambda_\sigma\right). \tag{24}$$

The continuum forward map $\mathbf{F}$ of section 2 is defined using this measurement operator as

$$\mathbf{F}(\sigma) = \mathrm{vec}(\mathcal{M}_n\left(\Lambda_\sigma\right)), \tag{25}$$

where $\mathrm{vec}(A)$ denotes the operation of stacking in a vector in $\mathbb{R}^g$, $g = n(n-1)/2$, the entries in the strict upper triangular part of a matrix $A \in \mathbb{R}^{n\times n}$. Because of reciprocity and conservation of currents, these entries completely determine the measured DtN map $\mathcal{M}_n\left(\Lambda_\sigma\right)$. Hence, another (equivalent) way of writing the compatibility condition (24) is

$$\mathbb{F}(\boldsymbol{\gamma}) = \mathbf{F}(\sigma). \tag{26}$$

where $\mathbb{F}(\boldsymbol{\gamma}) = \mathrm{vec}(\Lambda_{\boldsymbol{\gamma}})$ is the discrete forward map.

One possible choice of the measurement operator consists of taking point values of the kernel of Λ_σ. Its consistency with networks is shown in [27, 25]. Another choice, which we use in this paper, is to lump fluxes over disjoint segments of $\mathcal{B}$ that model electrode supports. Its consistency with networks is shown in [9, 23]. Such an operator is defined using the nonnegative "electrode" functions $\chi_1, \ldots, \chi_n$ in $H^{1/2}(\mathcal{B})$, with disjoint supports, numbered in circular order on $\mathcal{B}$. We normalize them to integrate to one on $\mathcal{B}$. The operator $\mathcal{M}_n$ maps Λ_σ to the symmetric matrix with off-diagonal entries given by

$$(\mathcal{M}_n(\Lambda_\sigma))_{i,j} = \langle \chi_i, \Lambda_\sigma \chi_j \rangle, \qquad i \neq j, \tag{27}$$

where $\langle \cdot, \cdot \rangle$ is the duality pairing between $H^{1/2}(\mathcal{B})$ and $H^{-1/2}(\mathcal{B})$. The diagonal entries are taken so that the rows (and columns) of $\mathcal{M}_n(\Lambda_\sigma)$ sum to zero. This way we avoid measuring the DtN map on the diagonal, where the kernel is singular. At the same time, such choice enforces the conservation of currents.

3.1.2. ***Solvability of the inverse problem for resistor networks.*** The question of solvability of the inverse problem for circular planar networks like $(\Gamma, \boldsymbol{\gamma})$ has been settled in [15, 16, 25, 18, 19]. The answer is that when the graph Γ is *critical*, the discrete forward map $\mathbb{F}$ is one-to-one, and there exists a left inverse $\mathbb{F}^{-1}$ so that $\mathbb{F}^{-1}(\mathbb{F}(\boldsymbol{\gamma})) = \boldsymbol{\gamma}$ for all $\boldsymbol{\gamma} > 0$. A graph is *critical* if it is *well connected* and if it does not contain any redundant edges. See [15, 16] for a technical definition of criticality and well-connectedness. In a critical network, the number n of boundary nodes and the number g of edges in the graph obey $g = n(n-1)/2$. This says that there are as many unknown conductances in the network as there are degrees of freedom in the DtN map $\Lambda_{\boldsymbol{\gamma}} \in \mathbb{R}^{n\times n}$.

It remains to define the graph of the network, so that it is critical, and thus uniquely determined by (24). Typically, different graph topologies are better suited for the full and partial data measurements. Here we use the topologies considered in [9, 23, 13, 32, 10], see Appendix B for details.

The inverse problem for critical networks $(\Gamma, \boldsymbol{\gamma})$ can be solved with at least two approaches. We use them both in our study of the nonlinear inverse problem in section 5.

1. **Layer peeling** [15, 13, 10]: A direct method giving the conductances $\boldsymbol{\gamma}$ in a finite number of algebraic operations. The advantage of layer peeling is that it is fast and explicit. The disadvantage is that it becomes quickly unstable, as the size of the network grows. Moreover, noisy data may not be consistent

with a network, i.e. the consistency relation (26) may not hold if the forward map $\mathbf{F}$ is noisy.

2. **Optimization:** Use standard optimization techniques to find conductances $\boldsymbol{\gamma}$ that best fit the (possibly noisy) measurements in the least squares sense (see section 4.2 for more details).

3.2. **Inversion on optimal grids.** We denote by $\sigma_\star$ the true conductivity, to distinguish it from the estimates that we denote generically by σ. The relations (22) between $\boldsymbol{\gamma}$ and $\sigma_\star$ have been derived in the discretization of the forward problem. We use them for the conductances of the network $(\Gamma, \boldsymbol{\gamma})$ recovered from the measurements $\mathbf{F}(\sigma_\star)$, in order to estimate $\sigma_\star$. This does not work unless we use a special grid in (22) [9, 11]. The idea behind the inversion on optimal grids is that the geometrical factors $L(\Sigma_{\alpha,\beta})/L(E_{\alpha,\beta})$ and the distribution of the points $P_{\alpha,\beta}$ in (22) depend weakly on σ. Therefore, we can determine both the geometrical factors and the grid nodes from the resistor network $(\Gamma, \boldsymbol{\gamma}^{(1)})$, with the same graph Γ as before, and $\mathbb{F}(\boldsymbol{\gamma}^{(1)}) = \mathbf{F}(1)$. These are the measurements of the DtN map for constant conductivity $\sigma \equiv 1$, that we can compute, and $\gamma^{(1)}_{\alpha,\beta} \approx L(\Sigma_{\alpha,\beta})/L(E_{\alpha,\beta})$. We obtain the pointwise estimates

$$\sigma(P_{\alpha,\beta}) \approx \frac{\gamma_{\alpha,\beta}}{\gamma^{(1)}_{\alpha,\beta}}, \tag{28}$$

that we place in Ω at points $P_{\alpha,\beta}$ determined from a sensitivity analysis of the DtN map, as we explain next.

3.2.1. ***The sensitivity functions and the optimal grids.*** The distribution of points $P_{\alpha,\beta}$ in Ω is *optimal* in the sense that

$$\mathbb{F}(\boldsymbol{\gamma}(\sigma)) = \mathbf{F}(\sigma) \tag{29}$$

for conductances $\boldsymbol{\gamma} = \boldsymbol{\gamma}(\sigma)$ related to the continuum σ as in (22), and for $\sigma \equiv 1$ (i.e., for $\boldsymbol{\gamma}(1) = \boldsymbol{\gamma}^{(1)}$). Each conductance γ_k is associated with a point $P_{\alpha,\beta}$, so we write $k = k(\alpha,\beta)$. We define the optimal grid points as the maxima of the sensitivity functions given below, evaluated at $\sigma \equiv 1$,

$$P_{\alpha,\beta} = \arg\max_{\mathbf{x}\in\Omega} (D_\sigma \gamma_{k(\alpha,\beta)})(\mathbf{x})\Big|_{\sigma\equiv 1}. \tag{30}$$

These are the points at which the conductances are most sensitive to changes in the conductivity.

To compute the sensitivity functions, we take derivatives in (29) with respect to σ, and obtain

$$D_\sigma \boldsymbol{\gamma} = \left(D_{\boldsymbol{\gamma}} \mathbb{F}(\boldsymbol{\gamma}(\sigma))\right)^{-1} D_\sigma \mathbf{F}(\sigma). \tag{31}$$

The left hand side is a vector-function from Ω to $\mathbb{R}^g$. Its $k-$th entry is the sensitivity of conductance γ_k with respect to changes of σ. The matrix $D_{\boldsymbol{\gamma}}\mathbb{F}(\boldsymbol{\gamma}(\sigma)) \in \mathbb{R}^{g\times g}$ is invertible [15]. The Jacobian $D_\sigma \mathbf{F}(\sigma)$ can be written in terms of the Green's function of the differential operator $u \to \nabla\cdot(\sigma\nabla u)$ with $u|_{\mathcal{B}} = 0$, and the "electrode" functions χ_i introduced in section 3.1.1. The calculation of the Jacobian is given in detail in [13, Section 4]. For a more in depth description of the optimal grids and sensitivity functions we refer the reader to [9, 23, 13, 32] and especially to the review in [10].

3.2.2. ***The estimate of the conductivity on optimal grids.*** What we have computed so far allows us to define an initial estimate $\sigma^o(\mathbf{x})$ of the conductivity, as the linear interpolation of the values (28), on the optimal grid defined by (30). Then, we improve the estimate using a Gauss-Newton iteration that minimizes the objective function

$$\mathcal{J}(\sigma) = \|\mathbb{Q}(\mathbf{F}(\sigma)) - \mathbb{Q}(\mathbf{d})\|_2^2 \tag{32}$$

over search conductivity functions $\sigma(\mathbf{x})$. Here the data vector is given as in (5) for the conductivity $\sigma_\star$ that we wish to find. The *reconstruction mapping* is

$$\mathbb{Q}(\mathbf{d}) := \mathrm{diag}(1/\boldsymbol{\gamma}^{(1)})\mathbb{F}^{-1}(\mathbf{d}), \tag{33}$$

and it involves solving the discrete inverse problem for a resistor network. The map $\mathbb{Q}$ computes the pointwise estimates (28) from the data $\mathbf{d}$. Therefore, $\sigma^o(\mathbf{x})$ is a linear interpolation of $\mathbb{Q}(\mathbf{d})$ on the optimal grid.

The objective function $\mathcal{J}(\sigma)$ is different than the usual output least squares data misfit $\|\mathbf{F}(\sigma) - \mathbf{d}\|_2^2$. We use $\mathbb{Q}$ in (32) as a *nonlinear preconditioner* of the forward map $\mathbf{F}$, as explained in detail in [9, 23]. It is because of this preconditioning, and the good initial guess $\sigma^o(\mathbf{x})$, that we can obtain close estimates of σ by minimizing $\mathcal{J}(\sigma)$ in [9, 23] and in this paper. The estimates are computed with a Gauss-Newton iteration that basically converges in one step [9, 23].

We enforce the positivity of σ by the change of variables $\kappa = \ln(\sigma)$, so that we work with the map

$$\mathbf{G}(\kappa) = \ln\left[\mathbb{Q}(\mathbf{F}(\exp(\kappa)))\right]. \tag{34}$$

The Gauss-Newton iteration that we use in the parametrization (19) is

$$\kappa_j = \kappa_{j-1} + \left(D_\kappa \mathbf{G}(\kappa_{j-1})\right)^\dagger \left[\ln[\mathbb{Q}(\mathbf{d})] - \mathbf{G}(\kappa_{j-1})\right], \quad j = 1, 2, \ldots, \tag{35}$$

with initial guess $\kappa_o = \ln(\sigma^o)$. The index $\dagger$ denotes the Moore-Penrose pseudo-inverse, and the iteration amounts to finding the update $\kappa_j - \kappa_{j-1}$ as the orthogonal projection of the residual onto the span of the sensitivities, the column space of the transpose of $D_\kappa \mathbf{G}(\kappa_{j-1})$. These sensitivities are easily related to those computed in section 3.2.1, using the chain rule to deal with the change of variables $\kappa = \ln(\sigma)$.

4. Numerical experiments setup.

We explain in section 4.1 how we simulate the noisy measurements. The noise may be too high for the layer peeling method to work. The optimization method presented in section 4.2 is more robust to noise and, as a bonus, it allows us to solve efficiently the optimization problem for the MAP estimate (10) with the resistor network discretization (see Remark 1). For reference, we include noiseless reconstructions in section 4.3.

4.1. Data and noise models.

We solve equation (1), with a second order finite volume method on a very fine, uniform, tensor product grid, with $N \gg n$ nodes on the boundary. In all our experiments we kept N fixed for each setup (full, one and two sided partial data problems). This approximates $\mathcal{M}_N(\Lambda_{\sigma_\star})$, where $\mathcal{M}_N$ is the measurement operator of section 3.1.1. The noise $\boldsymbol{\epsilon}$ in (5) is given by

$$\boldsymbol{\epsilon} = \mathrm{vec}\left(\mathcal{M}_n(\boldsymbol{\mathcal{E}})\right), \qquad \boldsymbol{\mathcal{E}} \in \mathbb{R}^{N\times N}. \tag{36}$$

We use two noise models, defined in terms of the noise level ℓ and a symmetric $N \times N$ matrix $\boldsymbol{\eta}$, with Gaussian, identically distributed entries with mean zero and variance one. The entries in $\boldsymbol{\eta}$ on and above the diagonal are uncorrelated. The

first model scales the noise by the entries of the DtN map for constant conductivity $\sigma \equiv 1$,

$$\boldsymbol{\mathcal{E}} = \ell\, \mathcal{M}_N(\Lambda_1) \cdot \boldsymbol{\eta}, \tag{37}$$

where symbol $\cdot$ stands for componentwise multiplication. The scaling makes the noise easier to deal with, and the model is somewhat similar to *multiplicative noise*. The second noise model is

$$\boldsymbol{\mathcal{E}} = \ell \frac{\boldsymbol{\eta}}{\|\boldsymbol{\eta}\|}, \tag{38}$$

where $\|\ \|$ is a matrix norm that approximates the continuum $H^{1/2}(\mathcal{B}) \to H^{-1/2}(\mathcal{B})$ operator norm. It is defined in Appendix C.

4.2. **The Gauss-Newton iteration for determining the resistor networks.** The direct, layer peeling algorithms described in [15, 13, 10] are fast, but highly unstable and can be used only for very small noise. It is not known how to regularize layer peeling algorithms. To deal with the instability, we can only reduce the size of the network, as was done in [9]. However, simply reducing the network size is not sufficient for the larger noise levels considered in the simulations. We use instead the more robust Gauss-Newton method described below, which allows regularization. The Gauss-Newton method is more expensive than layer peeling (about 20 times more expensive for $n = 7$), but the computational cost is reasonable because the dimension g of the vector of unknown conductances is small for noisy data, and the Jacobian is relatively inexpensive to compute.

The Gauss-Newton method determines the log-conductances $\boldsymbol{\kappa} = \ln(\boldsymbol{\gamma})$ in the network $(\Gamma, \boldsymbol{\gamma})$ (with topology Γ fixed) by minimizing the objective functional

$$\mathcal{O}(\boldsymbol{\kappa}) = (\mathbb{F}(\exp(\boldsymbol{\kappa})) - \mathbf{d})^T \mathcal{C}^{-1} (\mathbb{F}(\exp(\boldsymbol{\kappa})) - \mathbf{d}) + \alpha ||\boldsymbol{\kappa} - \boldsymbol{\kappa}_{\rm ref}||^2, \tag{39}$$

over $\boldsymbol{\kappa} \in \mathbb{R}^g$. Thus, the positivity of the conductances $\boldsymbol{\gamma} = \exp(\boldsymbol{\kappa})$ is satisfied automatically. The objective function (39) corresponds to a Gaussian prior on the log conductances $\boldsymbol{\kappa}$. The first term in (39) measures the misfit between the measured data $\mathbf{d}$ modeled by (5), and the data produced by a network with log-conductances $\boldsymbol{\kappa}$. Here $\mathcal{C}$ is the covariance matrix of the measurements. The second term in (39) is a Tikhonov type regularization penalizing the distance from some reference log-conductances $\boldsymbol{\kappa}_{\rm ref}$. The parameter $\alpha > 0$ determines the strength of the penalty term.

In our numerical experiments, the Gauss-Newton approximation of the Hessian of $\mathcal{O}(\boldsymbol{\kappa})$ is further regularized by adding $10^{-4}/\mathcal{C}_{1,1}$ to its diagonal. The iterations are stopped either when the norm of the gradient of $\mathcal{O}(\boldsymbol{\kappa})$ is 10^{-4} smaller than that at the initial iterate, or when the maximum number of iterations (300) is reached. The initial iterate is $\boldsymbol{\kappa} = \ln(\boldsymbol{\gamma}^{(1)})$, and we take as reference log-conductances $\boldsymbol{\kappa}_{\rm ref} = \ln(\boldsymbol{\gamma}^{(1)})$.

Remark 1. Recall from (18) that the network is the reduced model that matches the data. Therefore:

1. When $\alpha > 0$, finding log-conductances that minimize $\mathcal{O}(\boldsymbol{\kappa})$ is equivalent to finding the MAP estimate (10), with the resistor network based parametrization, and the prior (44). The regularization parameter α is the same in both (10) and (39). Moreover, when $\boldsymbol{\kappa}_{\rm ref} = \ln(\boldsymbol{\gamma}^{(1)})$ in (39), the reference parameters appearing in (44) are $\mathbf{s}_{\rm ref} = \mathbf{1}$ (vector of all ones with length g).

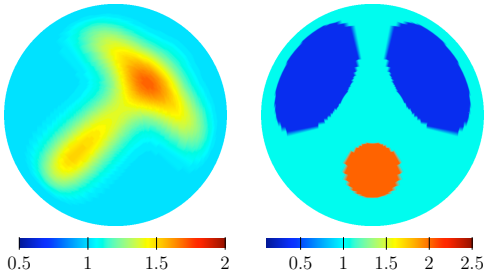

FIGURE 2. Conductivities used in the numerical experiments. Left: smooth conductivity. Right: piecewise constant chest phantom.

2. When $\alpha = 0$, minimizing $\mathcal{O}(\boldsymbol{\kappa})$ is equivalent to finding the MAP estimate (10) with the resistor network based parametrization and the upper/lower bound (42) (for a large enough upper bound $\sigma_{\max}$).

4.3. **Noiseless reconstructions.** We show in Figures 3 and 4 the reconstructions of the true smooth and piecewise constant conductivities displayed in Figure 2. The reconstructions are obtained in the full and partial boundary setups, and for noiseless data. Two distinct cases of partial boundary measurements are considered. In the *one-sided* case the accessible boundary $\mathcal{B}_A$ consists of a single connected segment of $\mathcal{B}$. In the *two-sided* case the accessible boundary $\mathcal{B}_A$ consists of two disjoint segments of $\mathcal{B}$.

We display in the top row of Figures 3 and 4 the initial guess $\sigma^o(\mathbf{x})$ of the Gauss-Newton iteration (35). It is the piecewise linear interpolation of the values $\sigma^o(P_{\alpha,\beta}) = \sigma_{k(\alpha,\beta)}$, where σ_k are obtained from (28), and the optimal grid nodes $P_{\alpha,\beta}$ are defined by (30). The function $\sigma^o(\mathbf{x})$ is linear on the triangles obtained by a Delaunay triangulation of the points $P_{\alpha,\beta}$. In the partial boundary measurements case we display $\sigma^o(\mathbf{x})$ in the subdomain delimited by the accessible boundary and the segmented arc connecting the innermost grid points. We set $\sigma^o(\mathbf{x})$ to the constant value one in the remainder of the domain. The plots in the bottom row in Figures 3 and 4 display the result of one step of the Gauss-Newton iteration described in section 3.2.2.

The network topologies are defined in Appendix B. The reconstructions from full boundary data are in the left column in Figures 3 and 4. They are obtained with a circular network $C\left(\frac{n-1}{2}, n\right)$, with $n = 29$. The reconstructions with the one-sided partial boundary measurements are in the middle column, and they are obtained with a pyramidal resistor network Γ_n, for $n = 16$. The reconstructions with the two-sided boundary measurements are in the right column. They are obtained with a resistor network T_n, for $n = 16$.

5. **Effect of parametrization on the reconstruction error.** We study numerically the effect of noise on the inversion with (a) resistor networks, and (b) the conductivity parametrized with piecewise linear basis functions. We consider in section 5.1 the linearized problem about the constant conductivity $\overline{\sigma} \equiv 1$, and in section 5.2 the nonlinear problem.

5.1. **The linearized problem.** The results in this section are for linearization at the constant conductivity $\overline{\sigma}(\mathbf{x}) \equiv 1$, with additive noise modeled as in (38). All

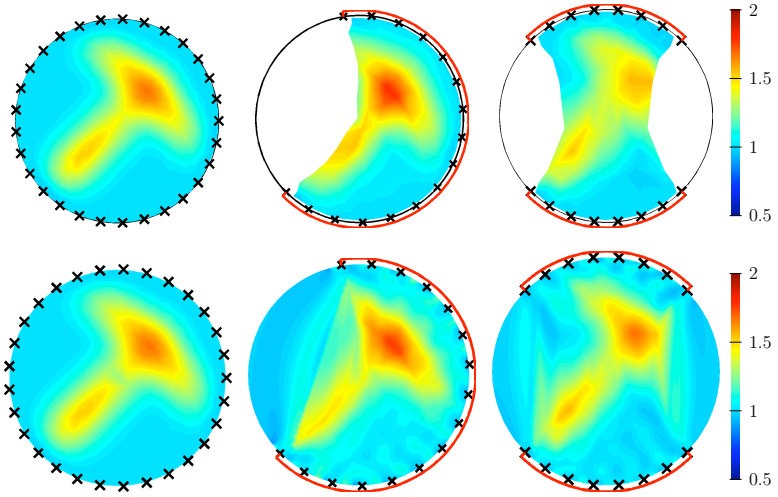

FIGURE 3. Reconstructions of the smooth conductivity with noiseless data.

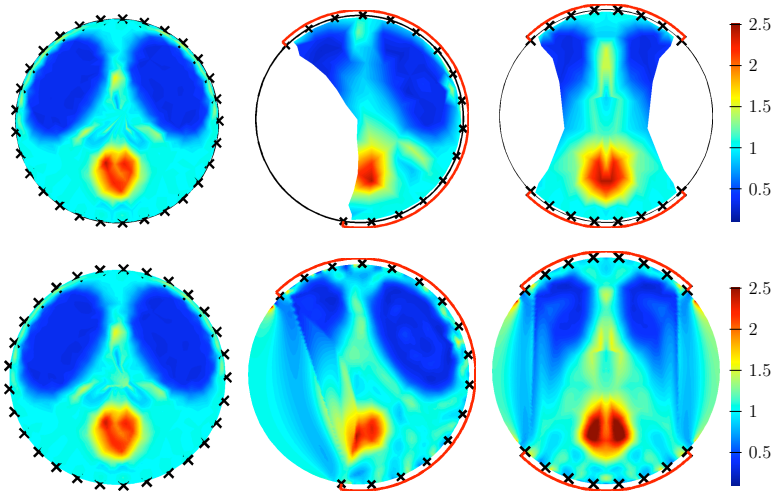

FIGURE 4. Reconstructions of the piecewise constant conductivity with noiseless data. Here and in Figure 3: Left column: full boundary measurements. Middle column: one-sided partial measurements. Right column: two-sided partial boundary measurements. The top row shows the initial guess $\sigma^o(\mathbf{x})$. The bottom row shows the result of one step of the Gauss-Newton iteration. The color scale is the same used for the true conductivity in Figure 2.

the three parametrizations described in section 2.2 represent exactly $\overline{\sigma} \equiv 1$, with a parameter vector $\mathbf{s}$ of all ones, i.e. $\mathcal{S}(\mathbf{1}) = 1$. Hence, the linearization of the forward map around $\overline{\mathbf{s}} = 1$ can be written as

$$\mathbf{F}(\mathcal{S}(\mathbf{1} + \delta\mathbf{s})) = \mathbf{F}(1) + D_\sigma \mathbf{F}(1) D_{\mathbf{s}} \mathcal{S}(\mathbf{1}) \delta\mathbf{s} + o(\delta\mathbf{s}), \tag{40}$$

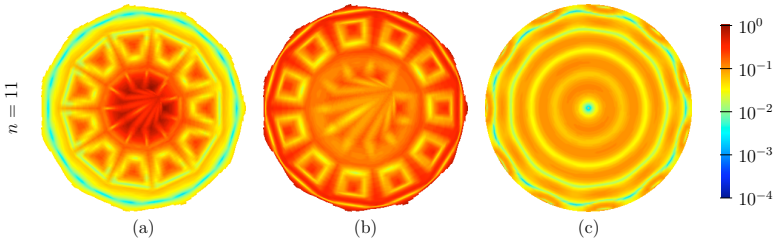

FIGURE 5. Standard deviation of reconstructions for the linearized problem. (a): Piecewise linear basis functions on uniform grid. (b): Piecewise linear basis functions on optimal grid. (c): Resistor network parametrization. The color scale is base-10 logarithmic and the noise level is $\ell = 0.01\%$ (additive noise model (38)). The circular resistor network has $n = 11$ boundary points and the noise $\boldsymbol{\mathcal{E}}$ is given at $N = 100$ equidistant points on the boundary.

for a small perturbation $\delta\mathbf{s}$ of the parameters. If we discretize the conductivity on a fine grid with N_σ points, the Jacobian $D_\sigma\mathbf{F}(1)$ is a $g \times N_\sigma$ matrix, and the Jacobian $D_\mathbf{s}\mathcal{S}(\mathbf{1})$ is an $N_\sigma \times g$ matrix with columns given by the basis functions ϕ_k in (17).

The estimate σ_{MAP} is calculated by solving the optimization problem (10), with the linearization (40) of the forward map, and the upper/lower bound prior (42). This optimization is a quadratic programming problem that we solve using the software QPC [38]. The mean and variance of σ_{MAP} are estimated with Monte Carlo simulations

$$\begin{aligned} \text{Var}[\sigma(\mathbf{x})] &\approx \frac{1}{M-1}\sum_{m=1}^{M}\left[\sigma_{\text{MAP}}^{(m)}(\mathbf{x}) - \langle\sigma(\mathbf{x})\rangle\right]^2, \\ \langle\sigma(\mathbf{x})\rangle &\approx \frac{1}{M}\sum_{m=1}^{M}\sigma_{\text{MAP}}^{(m)}(\mathbf{x}), \end{aligned} \tag{41}$$

using $M = 1000$ samples. We do not show the mean $\langle\sigma(\mathbf{x})\rangle$ because it is basically $\overline{\sigma}(\mathbf{x})$ for all the cases that we present below. The standard deviation $\{\text{Var}[\sigma(\mathbf{x})]\}^{1/2}$ is shown in Figure 5 for the case of full boundary measurements, and the three parametrizations described in section 2.2. The noise level is $\ell = 0.01\%$. We choose it so small to minimize the action of the positivity constraints imposed by the prior. Larger noise levels are considered later in the paper.

With the resistor network parametrization, the standard deviation is smaller and does not increase toward the center of the domain. Also there are no active positivity constraints. The random fluctuations of σ_{MAP} in Figure 5 (b) lie mostly within three standard deviations, and are much smaller than the background conductivity $\overline{\sigma} \equiv 1$.

The piecewise linear parametrization on the equidistant grid gives a large, order one standard deviation in the center of the domain. The positivity constraints are active in 81.6% of realizations. Surprisingly, the piecewise linear parametrization on the optimal grid is worse. Its standard deviation is large, of order one in most of the domain, and the positivity constraints are active in 61.1% realizations. This shows that it is not enough to distribute the parameters on the optimal grid.

The same conclusion can be reached from Figure 6, where we display the condition number of the matrix $D_\sigma\mathbf{F}(1)D_\mathbf{s}\mathcal{S}(\mathbf{1})$, as a function of the number n of boundary points. The condition number increases exponentially with n, as expected from

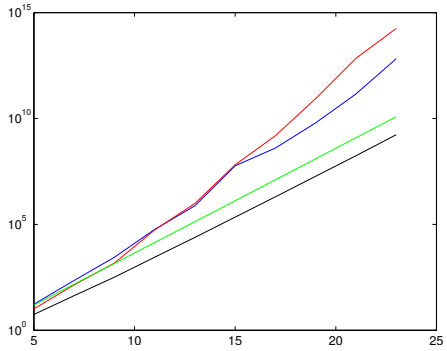

FIGURE 6. Comparison of the condition number of the matrix $D_\sigma \mathbf{F}(1) D_{\mathbf{s}} \mathcal{S}(\mathbf{1})$. The abscissa is the number n of boundary nodes and the ordinate is in logarithmic scale. The green line is for the fine grid forward map ($\mathcal{S}$ = identity). The red line is for the piecewise linear functions on the equidistant grid. The blue line is for the piecewise linear functions on the optimal grid. The black line is for the resistor network parametrization.

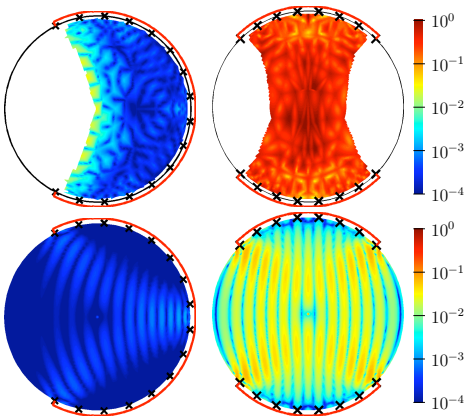

FIGURE 7. The standard deviation (base-10 log scale) for one-sided (left) and two-sided (right) boundary measurements. The resistor networks have $n = 16$ boundary points and the noise $\boldsymbol{\mathcal{E}}$ with level $\ell = 10^{-8}\%$ is given at $N = 83$ (left) and $N = 104$ (right) equidistant points on the accessible boundary. Top: piecewise linear parametrization on the optimal grid. Bottom: resistor network parametrization. The accessible boundary is in solid red.

the exponential ill-posedness of the problem. However, the rate of increase is smaller for the resistor network parametrization.

The standard deviation $\{\mathrm{Var}[\sigma(\mathbf{x})]\}^{1/2}$ is shown in Figure 7 for the case of one and two-sided boundary measurements. We use a much smaller noise level ($\ell = 10^{-8}\%$, additive model (38)) in the partial measurements case than in the full data case, because we compute the standard deviation for bigger networks ($n = 16$, same network size as in the reconstructions of Figures 3 and 4). Since the

condition number of the linearized problem grows exponentially as we increase n, only very small levels of noise can be used for $n = 16$. We present the results for the piecewise linear parametrization on the optimal grid (top row) and the resistor network parametrization (bottom row).

We reach the same conclusion as before. The resistor network parametrization gives a smaller standard deviation, that does not increase toward the inaccessible region. The piecewise linear parametrization on the optimal grid gives a large standard deviation near the inaccessible region in the one-sided case, and in the whole domain in the two-sided case. The positivity constraints are active in most realizations for the piecewise linear parametrization. They are not active for the resistor network parametrization.

5.2. **The nonlinear problem.** We study the statistics (mean and standard deviation) of the MAP estimates of the parameters $\mathbf{s}_{\text{MAP}}$ and the conductivities $\sigma_{\text{MAP}} = \mathcal{S}(\mathbf{s}_{\text{MAP}})$, which come from minimizing the functional (10). The study can be done for both the full and partial boundary measurement setup, but we present here only the full measurements case. We consider first, in section 5.2.1, very small noise so that we can use the fast layer peeling inversion algorithm to find the minimizer of (10), with resistor network parametrization and upper/lower bound prior (42). The speed of the algorithm allows us to compute the Cramér-Rao lower bound in a reasonable amount of time. We do not calculate the bound for larger noise, where we use regularized Gauss-Newton to determine the resistors, because of the computational cost. However, we do show in section 5.2.2 the bias and relative standard deviation of the reconstructions, and we also compare in section 5.2.3 the results to those with a piecewise linear discretization and Gaussian prior on the conductivity (43).

5.2.1. ***Statistics of resistor network inversion using layer peeling.*** The results in this section are for the MAP estimates $\mathbf{s}_{\text{MAP}}$, solving the optimization problem (10), with the resistor network parametrization, and upper/lower bound prior (42). We present the mean $\langle \mathbf{s} \rangle$, $\text{Bias}[\mathbf{s}] = \mathbf{s}_\star - \langle \mathbf{s} \rangle$, and the standard deviation $(\text{Var}[\mathbf{s}])^{1/2}$ of the estimates. We consider a very small noise level $\ell = 0.1\%$ (noise model (37)), so that we are able to minimize (39) with no regularization ($\alpha = 0$) directly, using the layer peeling algorithm.

Note that in the Cramér-Rao bound, the Fischer matrix (14) can be calculated analytically, but the bias factor (13) is estimated with Monte Carlo simulations. This is the expensive part of the computation, because we need a large number of samples to estimate the mean. In addition, each component of the vector $\mathbf{s}$ is perturbed to approximate the partial derivatives in (13) via finite differences. We use $M = 1000$ samples, and the bias is relative to $\mathbf{s}_\star$, the solution of the optimization problem (10) with noiseless data. The partial derivatives in (13) are approximated with finite differences with a step size of 0.01.

The bias factor is shown in Figure 8, and it is close to the identity matrix. That is to say, the estimates are unbiased. Figure 9 shows (a) the mean $\langle \mathbf{s} \rangle$, (b) $\text{Bias}[\mathbf{s}]$ and (c) the relative standard deviation $(\text{Var}[\mathbf{s}])^{1/2} / \langle \mathbf{s} \rangle$, where the division is understood componentwise. The last column (d) shows the difference in percentage between $\text{Var}[\mathbf{s}]$ and the Cramér-Rao bound in (12), normalized pointwise by the Cramér-Rao bound. We evaluate the Cramér-Rao bound by setting the bias factor (13) to the identity, which is a good approximation (recall Figure 8). Note that the difference between the variance and the Cramér-Rao bound is very small, indicating that the

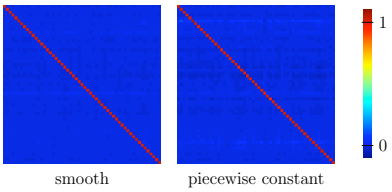

FIGURE 8. Estimated bias factor (13) for conductivities in Figure 2 is close to the identity.

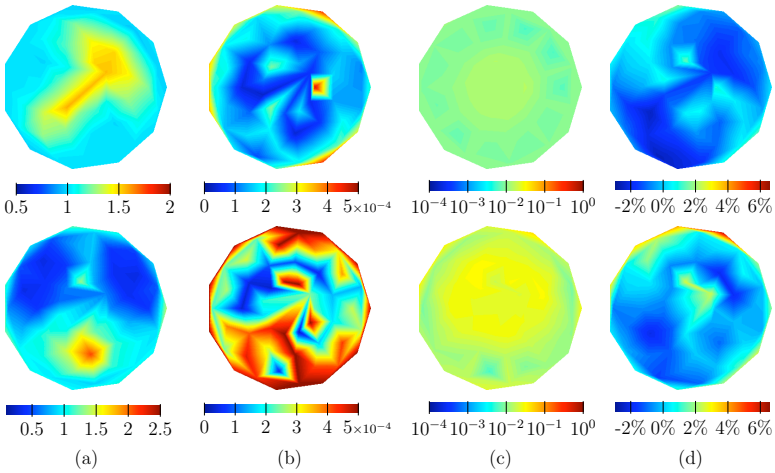

FIGURE 9. Results with the direct resistor finding algorithm: (a) mean, (b) absolute bias, (c) standard deviation relative to the mean, (d) relative difference between variance and Cramér-Rao bound relative to Cramér-Rao bound (in percentage). The noise model is (37) and the level is $\ell = 0.1\%$. The circular resistor network has $n = 11$ boundary points and the noise matrix $\boldsymbol{\mathcal{E}}$ is given at $N = 100$ equidistant points on $\mathcal{B}$. All parameters are linearly interpolated on the optimal grid.

estimation is efficient. The result in column (d) should be non-negative. We have some negative numbers, probably due to insufficient sampling in Monte Carlo, but they are so small in absolute value that we can treat them as essentially zero.

5.2.2. ***Statistics of conductivity estimates using optimization.*** Here we consider the additive noise model (38), with noise levels $\ell = 0.01\%$ and $\ell = 1\%$. These are the levels used in [30], and we use them to compare our results with those in [30]. Because solving (10) with only the upper/lower bound prior (42) does not give reliable estimates, we also use the prior (44). By Remark 1, this is equivalent to minimizing (39), which is computationally cheaper.

Figure 10 shows (a) the mean $\langle \sigma(\mathbf{x}) \rangle$, (b) Bias$[\sigma(\mathbf{x})]$ and (c) the relative standard deviation $(\text{Var}[\sigma(\mathbf{x})])^{1/2} / \langle \sigma(\mathbf{x}) \rangle$, for the noise level $\ell = 0.01\%$. The bias is computed with respect to $\sigma_\star$, the solution of the optimization problem (10), with noiseless data, no regularization ($\alpha = 0$), and a resistor network parametrization with $n = 11$ boundary nodes. The regularization parameter $\alpha = 10^{-6}$ is chosen so that both the bias and the relative standard deviation are small. The choice of the regularization

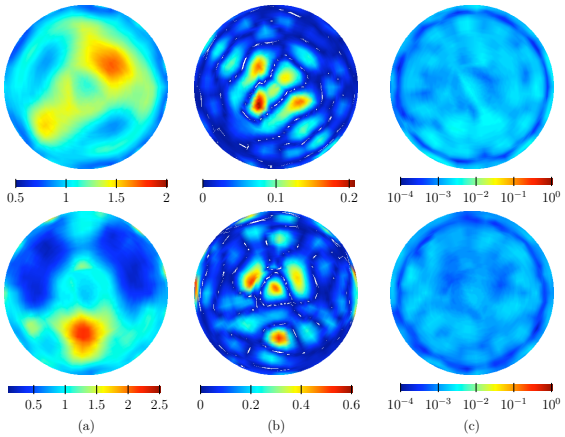

FIGURE 10. Results for $\ell = 0.01\%$ additive noise (38) and a regularization parameter $\alpha = 10^{-6}$ in (39). The circular resistor network has $n = 11$ boundary points and $\boldsymbol{\mathcal{E}}$ is given at $N = 100$ equidistant points on $\mathcal{B}$. Top: the smooth conductivity shown on the left in Figure 2. Bottom: the piecewise constant conductivity shown on the right in Figure 2. (a) mean, (b) bias, (c) relative standard deviation.

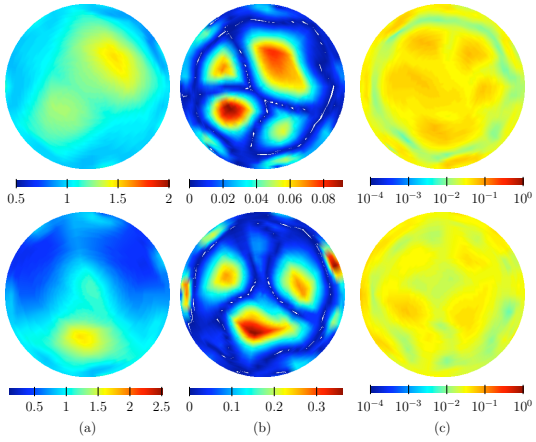

FIGURE 11. Results for $\ell = 1\%$ additive noise (38) and a regularization parameter $\alpha = 10^{-3}$ in (39). The circular resistor network has $n = 7$ boundary points and $\boldsymbol{\mathcal{E}}$ is given at $N = 100$ equidistant points on $\mathcal{B}$. Top: the smooth conductivity shown on the left in Figure 2. Bottom: the piecewise constant conductivity shown on the right in Figure 2.(a) mean, (b) bias, (c) relative standard deviation.

parameter is discussed in more detail in section 5.2.3. We do not show realizations of the MAP estimates, because they are close to the mean, as the standard deviation of the reconstructions is below 10^{-3}.

For the higher noise level $\ell = 1\%$, we present in Figure 11 the results for a smaller network, with $n = 7$ boundary nodes. Again we choose the regularization parameter

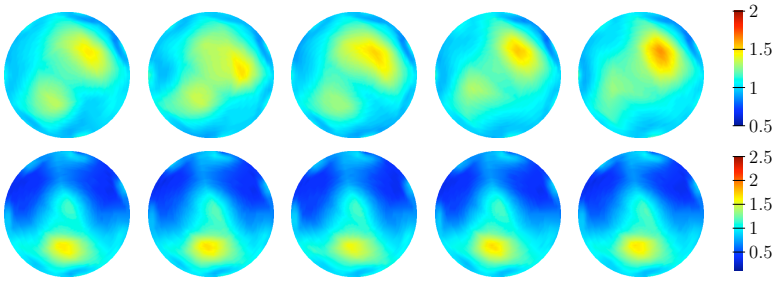

FIGURE 12. Realizations of $\sigma_{\text{MAP}}(\mathbf{x})$ for $n = 7$ boundary points, $\ell = 1\%$ additive noise (38) and regularization parameter $\alpha = 10^{-3}$ in (39).

$\alpha = 10^{-3}$ in such a way that both the bias and standard deviation are small. The relative standard deviation is less than 10%, and the realizations of $\sigma_{\text{MAP}}(\mathbf{x})$ shown in Figure 12 resemble the mean in Figure 11. These realizations are comparable to the reconstructions in [30]. The reconstructions with $n = 11$, noise level $\ell = 1\%$ and an appropriate choice of the regularization parameter are qualitatively similar to those with $n = 7$ shown in Figure 11, and thus are not included here.

5.2.3. ***Resistor network parametrization compared to other parametrizations.*** We now study the interplay between regularization and parametrization. We solve the optimization problem (10) with the three parametrizations of section 2.2. At the noise levels considered here, the same as in section 5.2.2, we need regularization to get reliable estimates of the conductivity. As was the case in section 5.2.2, the reconstructions with the resistor network parametrization are regularized with the prior (44). For the piecewise linear parametrizations, we regularize with the Gaussian prior (43), with reference conductivity $\sigma_{\text{ref}} \equiv 1$. Moreover, we stopped the iterations when either the maximum number of iterations (70) is reached, or when the norm of the gradient of the objective function at the current iterate is smaller by a factor of 10^{-4} than that at the initial iterate. We also added $10^{-8}/\mathcal{C}_{1,1}$ to the diagonal of the Gauss-Newton approximation to the Hessian. Recall that $\mathcal{C}$ is the covariance of the measurements.

We use two metrics to evaluate the reconstructions using different parametrizations. The first one is the L^2 norm of the true bias

$$\text{TrueBias}[\sigma] = \left(\int_\Omega (\sigma_\star(\mathbf{x}) - \langle \sigma(\mathbf{x}) \rangle)^2 d\mathbf{x} \right)^{1/2},$$

as a percent of the true conductivity $\sigma_\star$. This measures the *fidelity* (in average) of our reconstructions. The second metric is the L^2 norm of the standard deviation relative to L^2 norm of the mean of the reconstructions

$$\text{RelStd}[\sigma] = \frac{\left(\int_\Omega \text{Var}[\sigma(\mathbf{x})] d\mathbf{x} \right)^{1/2}}{\left(\int_\Omega \langle \sigma(\mathbf{x}) \rangle^2 \, d\mathbf{x} \right)^{1/2}},$$

which measures the *stability* of our reconstructions.

We report in Figure 13, for different values of the regularization parameter α, the true bias versus the relative standard deviation. Note the typical L-curve shape, which reflects the trade-off between accuracy (small bias) and stability (small standard deviation). When the regularization is not sufficient, the bias is small but the

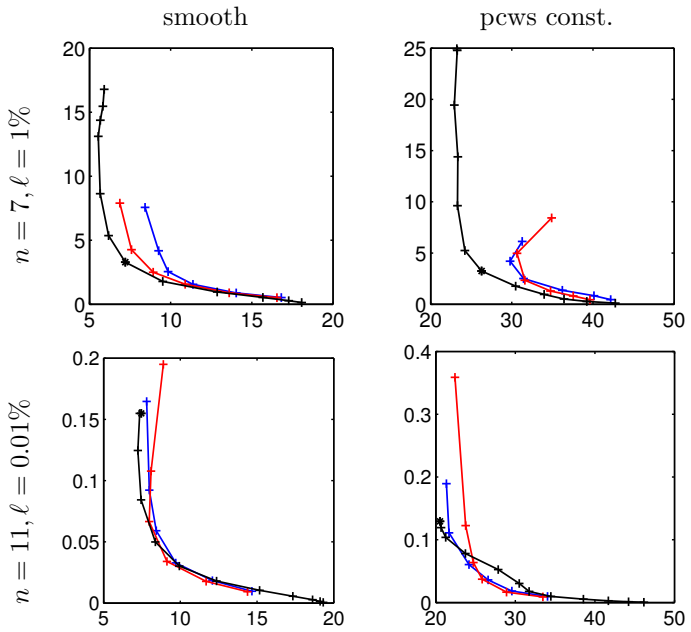

FIGURE 13. The true bias (in abscissa and in percent) against the relative standard deviation (in ordinate and in percent) for different values of the regularization parameter. The curves correspond to the resistor network approach (black), the linear interpolation on the optimal grid (blue) and the uniform grid (red). The number of realizations $N = 100$. The regularization parameter was $\alpha = 10^{-j/2}$, with $j = 1, 2, \ldots, 6$ for the linear interpolation (red and blue) and with $j = 1, 2, \ldots, 12$ for the network approach (black). The regularization parameter used for the reconstructions in figures 10 and 11 is indicated with a black star. Top: the smooth conductivity shown on the left in Figure 2. Bottom: the piecewise constant conductivity shown on the right in Figure 2.

standard deviation is large (vertical branch). When the problem is over regularized, the bias is large and the standard deviation is small (horizontal branch). The "best" choice of the regularization parameter would be near the "corner" of the L shape.

The first row in Figure 13 shows that for noise level $\ell = 1\%$ and for $n = 7$ boundary nodes, the resistor network parametrization outperforms the piecewise linear parametrizations: for a fixed standard deviation, the bias is smaller. This is specially noticeable for the piecewise constant conductivity. Interestingly, the uniform grid is slightly better than the optimal grid in this case. For $n = 11$ boundary nodes and $\ell = 0.01\%$ (second row), all approaches give comparable results, with the resistor network giving bias smaller by a few percent, specially if we allow a standard deviation above 0.1%.

Remark 2. We emphasize that the cost of solving (10) with the resistor network approach (i.e. solving (39)) is negligible compared to computing the Jacobian $D_{\mathbf{s}}\mathcal{S}(\mathbf{s})$. Thus, the resistor network approach takes about the same time as one step of Gauss-Newton to solve (10) with the piecewise linear parametrizations. In

the computations for Figure 13, the mean number of iterations for these linear parametrizations was at least 8, and varied depending on the regularization parameter, the grid and the conductivity. Therefore, the resistor network method is at least 8 times faster than the one using conventional discretization.

6. **Summary.** We presented a numerical study of the effects of noise on resistor based inversion algorithms. The algorithms were introduced in [9, 23, 12, 13, 32], and are briefly reviewed here. We have three measurements setups. The first assumes that the entire boundary $\mathcal{B}$ of the domain Ω is accessible. The other two are for partial boundary measurements confined to the accessible boundary $\mathcal{B}_A \subset \mathcal{B}$. One setup assumes one sided measurements, with $\mathcal{B}_A$ consisting of a segment of $\mathcal{B}$. The inversion algorithm is introduced in [13, 32]. The other setup is two sided, with $\mathcal{B}_A$ consisting of two disjoint segments of $\mathcal{B}$. The inversion amounts to defining a reconstruction mapping $\mathcal{S}(\mathbf{s})$, that takes a vector $\mathbf{s} = \boldsymbol{\gamma}/\boldsymbol{\gamma}^{(1)}$ of ratios of positive conductances of a network $(\Gamma, \boldsymbol{\gamma})$ and a reference network $(\Gamma, \boldsymbol{\gamma}^{(1)})$, to continuous conductivity functions defined in Ω. The network has a special graph Γ that is adapted to the measurement setup and which allows the conductors $\boldsymbol{\gamma}$ to be determined uniquely from measurements of the DtN map. The mapping $\mathcal{S}(\mathbf{s})$ involves a Gauss-Newton iteration that minimizes a preconditioned data misfit in the least-squares sense.

Our study considers three different parametrizations of the unknown conductivity with g degrees of freedom. The first two are piecewise linear interpolations on an equidistant grid and on the optimal grid, respectively. The third parametrization is based on resistor networks.

For the linearized problem, the piecewise linear parametrizations give large variances of the MAP estimates, even if we use the optimal grids. The resistor network parametrization is superior because the variances of the MAP estimates are lower and do not increase toward the inaccessible part of the domain.

The statistical study of the non-linear problem shows that when no additional prior (regularization) is introduced, and the noise is very small, using the resistor network parametrization gives reconstructions with small bias and the variance of the MAP estimates is very close to the optimal Cramér-Rao bound. For larger noise, we regularize the resistor based inversion with a prior on the conductances, and we compare the results with those of output least squares with piecewise linear parametrizations of the conductivity, on uniform and optimal grids and regularized with a Gaussian prior on the conductivity. The study assumes realistic noise levels [30]. All three parametrizations give a trade-off between accuracy (small bias) and statistical stability (small standard deviation of the estimates). However, the resistor based parametrization consistently outperforms the piecewise linear ones, giving a smaller bias for a fixed standard deviation in the reconstructions. The quality of the reconstructions is comparable to that in [30].

Our regularization priors are very simple. If additional prior information is available, the results of the resistor based inversion can be greatly improved, by enlarging the space of the Gauss-Newton iterates, beyond the span of the sensitivity functions of the reconstruction mapping. This was shown e.g. in [9, §7.1].

From the computational point of view, the inversion with resistor networks can be done at roughly the cost of one Gauss-Newton iteration for a conventional output least squares method, with the same number of degrees of freedom of the

parametrization. In our numerical experiments, the resistor network inversion was at least eight times faster.

Acknowledgments. The work of L. Borcea was partially supported by the National Science Foundation grants DMS-0934594, DMS-0907746 and by the Office of Naval Research grant N000140910290. The work of F. Guevara Vasquez was partially supported by the National Science Foundation grant DMS-0934664. The work of A. Mamonov was partially supported by the National Science Foundation grants DMS-0914465 and DMS-0914840. The authors were also partially supported by the National Science Foundation and the National Security Agency, during the Fall 2010 special semester on inverse problems at MSRI, Berkeley. We are grateful to Vladimir Druskin for sharing his deep insight of optimal grids.

Appendix A. Prior distributions.

(1) **Upper/lower bound prior**: We use this prior alone to explore the effect of the parametrization on the stability of the reconstructions, at small noise levels. It states that the conductivity and its inverse are bounded and positive. Let $\mathbb{S} = \{\mathbf{s} \in \mathbb{R}^g : \ [\mathcal{S}(\mathbf{s})](\mathbf{x}) \in (\sigma_{\min}, \sigma_{\max}), \quad \mathbf{x} \in \bar{\Omega}\}$ be the set of parameters mapped by $\mathcal{S}$ to positive conductivity functions bounded from below by $\sigma_{\min}$ and from above by $\sigma_{\max}$ in $\bar{\Omega}$. The prior is

$$\boldsymbol{\pi}_{\text{pr}}^{(UL)}(\mathbf{s}) = \frac{1_{\mathbb{S}}(\mathbf{s})}{|\mathbb{S}|}, \tag{42}$$

where $1_{\mathbb{S}}(\mathbf{s})$ is the indicator function that takes value one when $\mathbf{s} \in \mathbb{S}$, and zero otherwise, and $|\mathbb{S}|$ is the volume of $\mathbb{S}$. When we study maximum a posterior estimates of the conductivity in section 2.1, we set $\sigma_{\max}$ to a large enough value, and keep at the same time the number g of parameters low enough, for the constraint $[\mathcal{S}(\mathbf{s})](\mathbf{x}) \leq \sigma_{\max}$ to be automatically satisfied. However, we do enforce the positivity.

(2) **Gaussian prior on the conductivity**: This is a Tikhonov regularization prior that is useful at higher noise levels [29, Chapter 3]. It says that in addition to the conductivity being positive and bounded, we assume that σ has a normal distribution with mean σ_{ref}. The fluctuations $\mathcal{S}(\mathbf{s}) - \sigma_{\text{ref}}$ are uncorrelated from point to point, and the pointwise variance is α^{-1}. The prior is defined by

$$\boldsymbol{\pi}_{\text{pr}}^{(GC)}(\mathbf{s}) \sim \boldsymbol{\pi}_{\text{pr}}^{(UL)}(\mathbf{s}) \exp[-(\alpha/2)\|\mathcal{S}(\mathbf{s}) - \sigma_{\text{ref}}\|^2_{L^2(\Omega)}], \tag{43}$$

where the symbol "$\sim$" means equality up to a positive, multiplicative constant.

(3) **Prior on the parameters**: This is also a Tikhonov type regularization prior that is useful at higher noise levels. It says that in addition to the conductivity being positive and bounded, the vector of the logarithm of the parameters $\mathbf{s}$ is normally distributed, with mean $\log(\mathbf{s}_{\text{ref}})$ and covariance $\alpha^{-1}I$, where I is the $g \times g$ identity matrix,

$$\boldsymbol{\pi}_{\text{pr}}^{(GP)}(\mathbf{s}) \sim \boldsymbol{\pi}_{\text{pr}}^{(UL)}(\mathbf{s}) \exp[-(\alpha/2)\|\log(\mathbf{s}) - \log(\mathbf{s}_{\text{ref}})\|_2^2]. \tag{44}$$

Appendix B. Resistor network topologies.

Resistor networks $(\Gamma, \boldsymbol{\gamma})$ with *circular* graphs $\Gamma = C(l, n)$ are natural reduced models of the problem with full boundary measurements. The notation $C(l, n)$ [16, 17] indicates that the graph has l layers, and n edges in each layer. The edges may be in the radial direction, or transversal to it, as illustrated in Figure 14. For the network to be critical, and

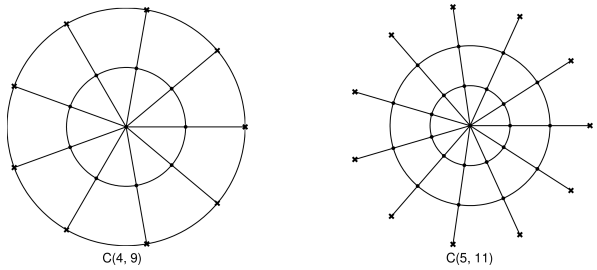

FIGURE 14. Circular resistor networks $C(l,n)$ with critical graphs: $l=(n-1)/2$. The interior nodes are indicated with dots and the boundary nodes with crosses.

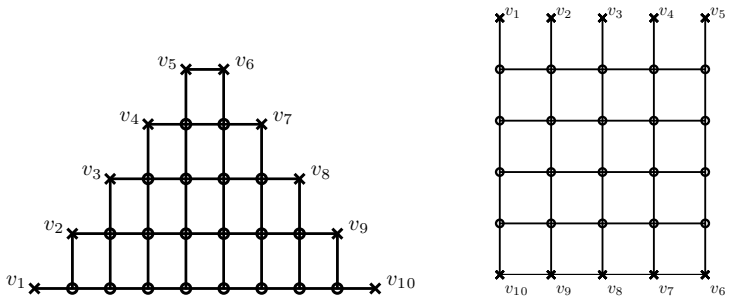

FIGURE 15. Resistor networks used for partial boundary measurements. Left: pyramidal network Γ_n. Right: two-sided network T_n. The boundary nodes v_j, $j=1,\dots,n$, $n=10$ are numbered in circular order and are indicated by $\times$. The interior nodes are indicated with $\circ$.

thus uniquely determined by $\mathbb{F}(\boldsymbol{\gamma})=\mathbf{F}(\sigma)$, we must nave n odd and $l=(n-1)/2$ [17, Proposition 2.3, Corollary 9.4], [9, Theorem 2].

For the one-sided partial boundary measurements we use a different network topology. While conformal or extremal quasiconformal coordinate transformations allow for circular networks to be used in the partial measurements case [12], the networks with *pyramidal* graphs $\Gamma=\Gamma_n$ are more natural [13]. They are shown in Figure 15 (left). The pyramidal networks are critical and thus uniquely recoverable [13]. They are natural to use with one-sided partial measurements because the sides of the pyramid, where the boundary nodes lie, can be mapped to the accessible segment $\mathcal{B}_A$ of the boundary. The base of the pyramid consists of interior nodes. They model the lack of penetration of the currents in the part of the domain near $\mathcal{B}_I$, the inaccessible boundary.

The inversion in the two-sided case is based on *two-sided* resistor networks [10] with graph denoted by $\Gamma=T_n$, and $n=2m$ boundary nodes. There are m nodes on each segment of the accessible boundary separated by the leftmost and rightmost interior nodes, as illustrated in the right plot in Figure 15. These interior nodes model the lack of penetration of the currents in the parts of the domain close to the inaccessible boundary. The two-sided network is critical and thus can be recovered with e.g. layer peeling [10].

Appendix C. **The norm used in the noise model.** Since the boundary $\mathcal{B}$ is the unit circle, we associate it with the angle interval $[0, 2\pi]$. Consider the Fourier series operator $\mathcal{U} : \ell^2 \to L^2[0, 2\pi]$, defined by

(45)
$$(\mathcal{U}\widehat{f})(\theta) = \frac{1}{\sqrt{2\pi}} \sum_{k=-\infty}^{\infty} \widehat{f}(k) e^{ik\theta}, \text{ and its adjoint } (\mathcal{U}^\star f)(k) = \frac{1}{\sqrt{2\pi}} \int_0^{2\pi} d\theta\, f(\theta) e^{-ik\theta}.$$

The fractional Sobolev norm H^s of f can be written as a weighted ℓ^2 norm $\| \ \|_2$,

$$\|f\|_{H^s} = \|W^s \mathcal{U}^\star f\|_2, \text{ where } (W^s \widehat{v})_k = \left(1 + k^2\right)^{s/2} \widehat{v}(k), \qquad k \in \mathbb{Z}. \tag{46}$$

The operator norm of a linear operator $A : H^{1/2}(\mathcal{B}) \to H^{-1/2}(\mathcal{B})$ is

$$\begin{aligned} \|A\|_{H^{1/2}(\mathcal{B}) \to H^{-1/2}(\mathcal{B})} &= \sup_{f \neq 0, f \in H^{1/2}} \frac{\|W^{-1/2} \mathcal{U}^\star f\|_2}{\|W^{1/2} \mathcal{U}^\star f\|_2} \\ &= \sup_{g \neq 0, g \in \ell^2} \frac{\|W^{-1/2} \mathcal{U}^\star A \mathcal{U} W^{-1/2} g\|_2}{\|g\|_2}. \end{aligned} \tag{47}$$

In particular, when $A = \Lambda_1$ we have $\Lambda_1 = \mathcal{U} K \mathcal{U}^\star$, where $K\widehat{v}(k) = |k|\widehat{v}(k)$. Thus $\|\Lambda_1\|_{H^{1/2} \to H^{-1/2}} = 1$.

We approximate the operator norm (47) by the norm $\| \ \|$, as follows. In an abuse of notation, let Λ_σ and Λ_1 be the restrictions of the continuum DtN maps to the N uniformly distributed fine grid points on $\mathcal{B}$. Consider the spectral decomposition

$$\frac{2\pi}{N} \Lambda_1 = U \Sigma U^\star, \qquad U^\star U = I. \tag{48}$$

The approximate norm is given by

$$\|\Lambda_\sigma\| = \sup_{g \neq 0, g \in \mathbb{R}^N} \frac{2\pi}{N} \frac{\|(I + \Sigma^2)^{-1/4} U^\star \Lambda_\sigma U (I + \Sigma^2)^{-1/4} g\|_2}{\|g\|_2}, \tag{49}$$

which is equivalent to finding the largest eigenvalue in magnitude of the matrix appearing in the numerator above. By construction, we have $\|\Lambda_1\| = 1$.

REFERENCES

[1] G. Alessandrini, *Stable determination of conductivity by boundary measurements*, Applicable Analysis, **27** (1988), 153–172.

[2] G. Alessandrini and S. Vessella, *Lipschitz stability for the inverse conductivity problem*, Advances in Applied Mathematics, **35** (2005), 207–241.

[3] H. B. Ameur, G. Chavent and J. Jaffré, *Refinement and coarsening indicators for adaptive parametrization: Application to the estimation of hydraulic transmissivities*, Inverse Problems, **18** (2002), 775–794.

[4] H. B. Ameur and B. Kaltenbacher, *Regularization of parameter estimation by adaptive discretization using refinement and coarsening indicators*, Journal of Inverse and Ill Posed Problems, **10** (2002), 561–584.

[5] K. Astala, L. Päivärinta and M. Lassas, *Calderón's inverse problem for anisotropic conductivity in the plane*, Communications in Partial Differential Equations, **30** (2005), 207–224.

[6] S. Asvadurov, V. Druskin and L. Knizhnerman, *Application of the difference Gaussian rules to solution of hyperbolic problems*, Journal of Computational Physics, **158** (2000), 116–135.

[7] J. A. Barcelo, T. Barcelo and A. Ruiz, *Stability of the inverse conductivity problem in the plane for less regular conductivities*, Journal of Differential Equations, **173** (2001), 231–270.

[8] L. Borcea and V. Druskin, *Optimal finite difference grids for direct and inverse Sturm-Liouville problems*, Inverse Problems, **18** (2002), 979–1002.

[9] L. Borcea, V. Druskin and F. Guevara Vasquez, *Electrical impedance tomography with resistor networks*, Inverse Problems, **24** (2008), 035013, (31pp).

[10] L. Borcea, V. Druskin, F. Guevara Vasquez and A. V. Mamonov, *Resistor network approaches to electrical impedance tomography*, Inverse Problems and Applications: Inside Out II, Mathematical Sciences Research Institute Publications, Cambridge University Press, **60** (2012), 55–118.

[11] L. Borcea, V. Druskin and L. Knizhnerman, *On the continuum limit of a discrete inverse spectral problem on optimal finite difference grids*, Communications on Pure and Applied Mathematics, **58** (2005), 1231–1279.

[12] L. Borcea, V. Druskin and A. V. Mamonov, *Circular resistor networks for electrical impedance tomography with partial boundary measurements*, Inverse Problems, **26** (2010), 045010.

[13] L. Borcea, V. Druskin, A. V. Mamonov and F. Guevara Vasquez, *Pyramidal resistor networks for electrical impedance tomography with partial boundary measurements*, Inverse Problems, **26** (2010), 105009.

[14] R. M. Brown and G. Uhlmann, *Uniqueness in the inverse conductivity problem for nonsmooth conductivities in two dimensions*, Commun. Partial Diff. Eqns., **22** (1997), 1009–1027.

[15] E. Curtis, E. Mooers and J. A. Morrow, *Finding the conductors in circular networks from boundary measurements* RAIRO - Mathematical Modelling and Numerical Analysis, **28** (1994), 781–814.

[16] E. B. Curtis, D. Ingerman and J. A. Morrow, *Circular planar graphs and resistor networks*, Linear Algebra and its Applications, **23** (1998), 115–150.

[17] E. B. Curtis and J. A. Morrow, "Inverse Problems for Electrical Networks," World Scientific, 2000.

[18] Y. C. de Verdière, *Reseaux electriques planaires I*, Commentarii Mathematici Helvetici, **69** (1994), 351–374.

[19] Y. C. de Verdière, I. Gitler and D. Vertigan, *Reseaux electriques planaires II*, Commentarii Mathematici Helvetici, **71** (1996), 144–167.

[20] V. Druskin and L. Knizhnerman, *Gaussian spectral rules for second order finite-difference schemes*, Numerical Algorithms, **25** (2000), 139–159.

[21] V. Druskin and L. Knizhnerman, *Gaussian spectral rules for the three-point second differences: I. A two-point positive definite problem in a semi-infinite domain*, SIAM Journal on Numerical Analysis, **37** (2000), 403–422.

[22] B. G. Fitzpatrick, *Bayesian analysis in inverse problems*, Inverse problems, **7** (1991), 675–702.

[23] F. Guevara Vasquez, "On the Parametrization of Ill-posed Inverse Problems Arising from Elliptic Partial Differential Equations," PhD thesis, Rice University, Houston, TX, USA, 2006.

[24] O. Y. Imanuvilov, G. Uhlmann and M. Yamamoto, *Global uniqueness from partial Cauchy data in two dimensions*, Arxiv preprint `arXiv:0810.2286`, (2008).

[25] D. Ingerman, *Discrete and continuous Dirichlet-to-Neumann maps in the layered case*, SIAM Journal on Mathematical Analysis, **31** (2000), 1214–1234.

[26] D. Ingerman, V. Druskin and L. Knizhnerman, *Optimal finite difference grids and rational approximations of the square root I. Elliptic problems*, Communications on Pure and Applied Mathematics, **53** (2000), 1039–1066.

[27] D. Ingerman and J. A. Morrow, *On a characterization of the kernel of the Dirichlet-to-Neumann map for a planar region*, SIAM Journal on Applied Mathematics, **29** (1998), 106–115.

[28] D. Isaacson, *Distinguishability of conductivities by electric current computed tomography*, IEEE transactions on medical imaging, **5** (1986), 91–95.

[29] J. P. Kaipio and E. Somersalo, "Statistical and Computational Inverse Problems," Springer Science+ Business Media, Inc., 2005.

[30] K. Knudsen, M. Lassas, J. L. Mueller and S. Siltanen, *Regularized d-bar method for the inverse conductivity problem*, Inverse Problems and Imaging, **3** (2009), 599–624.

[31] H. R. MacMillan, T. A. Manteuffel and S. F. McCormick, *First-order system least squares and electrical impedance tomography*, SIAM Journal on Numerical Analysis, **42** (2004), 461–483.

[32] A. V. Mamonov, "Resistor Networks and Optimal Grids for the Numerical Solution of Electrical Impedance Tomography with Partial Boundary Measurements," Ph.D thesis, Rice University, Houston, TX, USA, 2010.

[33] N. Mandache, *Exponential instability in an inverse problem for the Schrodinger equation*, Inverse Problems, **17** (2001), 1435–1444.

[34] A. I. Nachman, *Global uniqueness for a two-dimensional inverse boundary value problem*, Annals of Mathematics, (1996), 71–96.
[35] Ch. Pommerenke, "Boundary Behaviour of Conformal Maps," **299** of Grundlehren der Mathematischen Wissenschaften [Fundamental Principles of Mathematical Sciences], Springer-Verlag, Berlin, 1992.
[36] M. J. Schervish, "Theory of Statistics," Springer, 1995.
[37] A. D. Seagar, "Probing with Low Frequency Electric Currents," Ph.D thesis, University of Canterbury, UK. Department of Electrical Engineering, 1983.
[38] A. G. Wills and B. Ninness, "QPC - Quadratic Programming in C," Webpage, http://sigpromu.org/quadprog/.

Received December 2011; revised January 2013.

E-mail address: borcea@rice.edu
E-mail address: fguevara@math.utah.edu
E-mail address: mamonov@ices.utexas.edu